ORIGINAL ARTICLE

3D Printed Gene-activated Octacalcium Phosphate Implants for Large Bone Defects Engineering

Ilya Y. Bozo[1,2], Roman V. Deev[2,3], Igor V. Smirnov[4], Alexander Yu. Fedotov[4], Vladimir K. Popov[5], Anton V. Mironov[5], Olga A. Mironova[5], Alexander Yu. Gerasimenko[6,7], Vladimir S. Komlev[4,5]*

[1]Department of Maxillofacial Surgery, A.I. Burnazyan Federal Medical Biophysical Center, FMBA of Russia, Moscow, Russia

[2]Research and Development Department, Human Stem Cells Institute, Moscow, Russia

[3]Department of Pathology, I.I. Mechnikov North-Western State Medical University, Saint-Petersburg, Russia

[4]A.A. Baikov Institute of Metallurgy and Materials Science, Russian Academy of Sciences, Moscow, Russia

[5]Institute of Photon Technologies of Federal Scientific Research Centre "Crystallography and Photonics," Russian Academy of Sciences, Moscow, Russia

[6]Institute for Bionic Technologies and Engineering, I.M. Sechenov First Moscow State Medical University, Moscow, Russia

[7]Institute of Biomedical Systems, National Research University of Electronic Technology, Moscow, Russia

Abstract: The aim of the study was the development of three-dimensional (3D) printed gene-activated implants based on octacalcium phosphate (OCP) and plasmid DNA encoding *VEGFA*. The first objective of the present work involved design and fabrication of gene-activated bone substitutes based on the OCP and plasmid DNA with *VEGFA* gene using 3D printing approach of ceramic constructs, providing the control of its architectonics compliance to the initial digital models. X-ray diffraction, scanning electron microscopy (SEM), Fourier transform infrared spectroscopy, and compressive strength analyses were applied to investigate the chemical composition, microstructure, and mechanical properties of the experimental samples. The biodegradation rate and the efficacy of plasmid DNA delivery *in vivo* were assessed during standard tests with subcutaneous implantation to rodents in the next stage. The final part of the study involved substitution of segmental tibia and mandibular defects in adult pigs with 3D printed gene-activated implants. Biodegradation, osteointegration, and effectiveness of a reparative osteogenesis were evaluated with computerized tomography, SEM, and a histological examination. The combination of gene therapy and 3D printed implants manifested the significant clinical potential for effective bone regeneration in large/critical size defect cases.

Keywords: Three-dimensional printing, Bone tissue engineering, Calcium phosphate, Octacalcium phosphate, Gene, Plasmid DNA, Vascular endothelial growth factor.

***Corresponding Author:** Vladimir S. Komlev, A.A. Baikov Institute of Metallurgy and Materials Science, Russian Academy of Sciences, Moscow, Russia; komlev@mail.ru

***Received*:** March 10, 2020; ***Accepted*:** April 14, 2020; ***Published Online*:** June 03, 2020

(This article belongs to the *Special Section: Bioprinting in Russia*)

Citation: Bozo IY, Deev RV, Smirnov IV, *et al*., 2020 3D Printed Gene-activated Octacalcium Phosphate Implants for Large Bone Defects Engineering. *Int J Bioprint*, 6(3): 275. DOI: 10.18063/ijb.v6i3.275.

1 Introduction

Skeletal bone disorder caused by traumas, inflammation, malignancies, intervertebral disk disease, as well as alveolar ridge atrophy following tooth loss is highly prevalent and incrementally increasing[1]. Despite the development of numerous ordinary and activated bone substitutes, the management of large bone defects is still challenging and usually demands the use of bone autografts that is associated with a certain complication rate, donor site morbidity,

contraindications, a considerable duration of the intervention, and post-surgery rehabilitation[2]. This creates a strong need for acceptable alternative of bone autografts in clinical practice. Biodegradable implants possesing chemical composition, structure, osteoconductive and osteoinductive potential corresponding to native bone, with shape and sizes exactly conforming to the parameters of substitute for specific bone defect could become such an alternative. In addition, a personalized bone substitute should have optimal biomechanical properties allowing at least its stable fixation *in situ* with standard, for example, metal constructions.

Three-dimensional (3D) printing techniques that facilitate development of custom-made medical devices are the most promising approach to solve the problems in personalized bone reconstruction. However, in selecting the material for 3D printing, scientists frequently make their decision based on technical feasibility of additive manufacturing with a high spatial resolution rather than on the potential of a biomaterial to actually improve reparative osteogenesis. Therefore, some polymer materials such as polycaprolactone[3] and polylactic-co-glycolic acid[4], which are greatly suitable for 3D printing including that associated with addition of biologically active components (living cells, growth factors, etc.), but less effective for bone grafting[5] are taken often. On the other hand, natural and synthetic analogues of bone matrix components with optimal biomechanical properties show that osteoconduction and biodegradable property through the release of components that cells can utilize to produce and mineralize the intercellular matrix are more appropriate for bone regeneration[6]. For instance, octacalcium phosphate (OCP) has optimal osteoconductive properties and biodegradation rate. It is a precursor of natural mineral component of the bone matrix[7], and it stimulates differentiation of multipotent mesenchymal stromal cells to osteogenic lineage[8]. However, it is very difficult to achieve a high spatial resolution in 3D printing of ceramic implants, and the problem becomes even more irresistible if some biologically active components are needed to enhance osteoinductive capacity required to restore large bone defects that are characterized by "osteogenic insufficiency"[9].

Cells and growth factors are most actively employed osteoinducing factors for 3D printed scaffolds[10]. However, cells require oxygenation that limits their possible use in creating personalized tissue engineering constructions or bioactive implants of large sizes, whereas growth factors are short-lived and short-distant[9]. Gene-activated materials are devoid of these drawbacks, though the delivery of gene constructs in the safest, a non-viral, variant is "Achilles heel" of the approach[9].

In this study, based on our previous experience in 3D printing of OCP bone substitutes[11,12], considering the critical role of angiogenesis for reparative osteogenesis, we hypothesized that deposition of plasmid DNA carrying a gene of vascular endothelial growth factor (pDNA-*VEGFA*), as an active substance of the "Neovasculgen" drug (developed and certified for clinical applications by HSCI, Russia)[13], into custom-made OCP-based 3D printed implants would make it effective in large bone defect substitution and guided bone regeneration.

2 Experimental method

2.1 Materials

Initial tricalcium phosphate (TCP) powder was produced in an aqueous medium by slowly adding diammonium phosphate ($(NH_4)_2HPO_4$) solution into calcium nitrate ($Ca(NO_3)_2 4H_2O$) solution, containing NH_4OH. Fraction of TCP agglomerated particles with mean size in diameter 40 – 80 μm was selected as a row material for all further experiments. 1.0% aqueous solution of salts of phosphoric acid (pH value equals 4.75) was utilized as "ink" for 3D printing[11]. All used reagents were ordered and received from Sigma-Aldrich (USA).

2.2 3D printing

3D printed samples were made under a previously modified printing algorithm of ceramic constructions described elsewhere in details[12].

Layer-by-layer printing process of 3D ceramics scaffolds was performed on custom-made 3D printer (shown in **Figure 1** and presented on Supplementary Video 1). The approach of 3D printing is based on a route, which allowed chemical reaction between TCP agglomerated particles and "ink" (diluted phosphoric acid). The schematic set up of the custom-made 3D printer is shown in **Figure 1A and B**.

There were several models prepared in our work: non-porous disks with diameter of 10-mm and thickness of 2-mm to assess baseline biodegradation and mechanical properties; disks with 10-mm diameter, 2-mm thickness, and a net-like structure to evaluate the efficacy of gene constructs delivery and custom-made implants with a complex architectonics exactly corresponding to the planned defect substitution in adult pig mandibular (**Figure 1 C1**) and tibia (**Figure 1 C2**), followed by bone reconstruction.

3D models were made in the form of disks with standard tools in a Blender software (Blender Foundation, Germany). In the bone reconstruction experiment, multispiral medical computerized tomography (CT) of the skull and hindlimb of adult pig with a weight of 50 kg was done. Then, planned bone defects were mapped in computerized images using 3D slicer software (Brigham and Women's Hospital, Inc., USA). These were a segmental "T-shaped" defect of the tibia diaphysis with a total length of 30 mm including 10 mm circular central part for complete

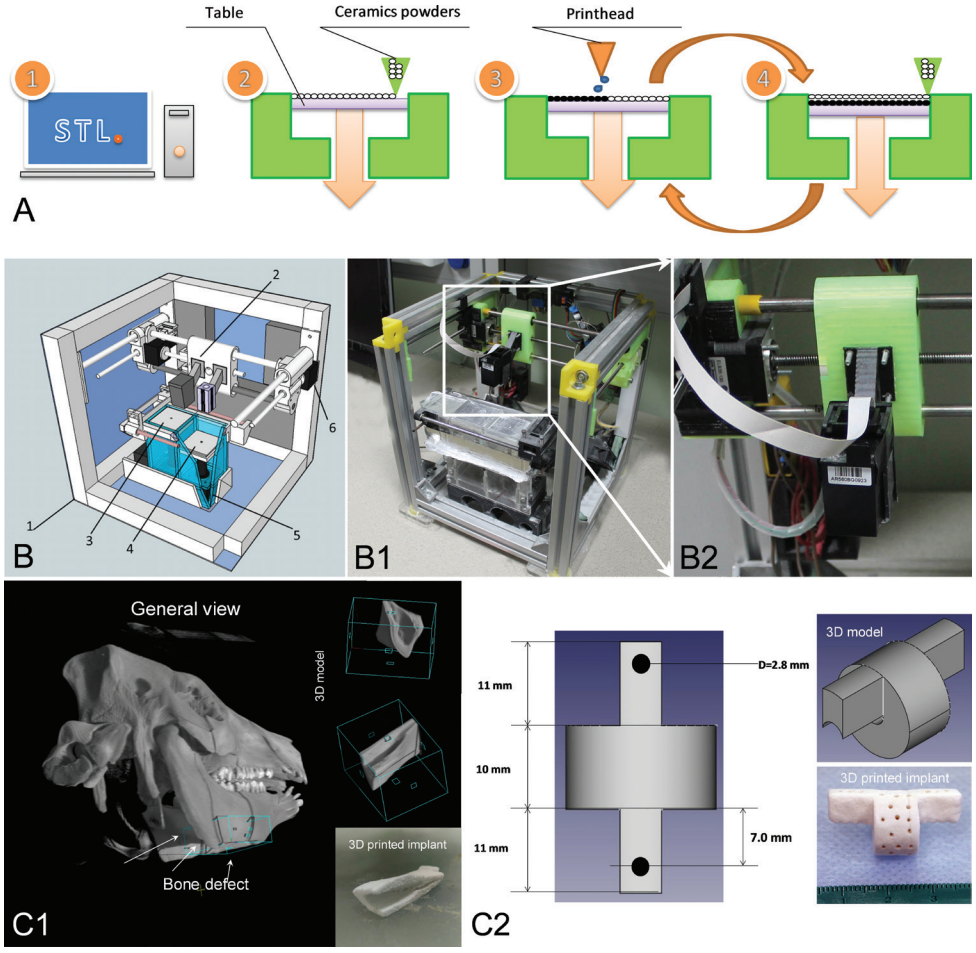

Figure 1. (A) Schematic overview of the three-dimensional (3D) printing approach; (B) Custom-made 3D printer: (1) 3D printer frame; (2) printing head; (3) stuffer with spreader; (4) Z-piston; (5) building box; (6) stepper motors. (B1, B2) Custom-made 3D printer and printing head; (C1, C2) 3D planned defects for mandibular and pig tibia.

disintegration and branching proximal and distal cortical defects of the diaphyseal anterior surface sized 10 × 5 × 5 mm^3 each; a full-layer defect of the mandible lower edge from the angle to the front sized 25 × 15 × 10 mm^3. The specified zones were segmented with the removal of surrounding tissues. 3D reconstructions of designated bone regions, corresponding to the planned bone defects were transferred into MeshLab (Visual Computing Lab, Italy), a mesh-object was generated, transferred into Blender and the implant structure was corrected, i.e. irregularities were removed, perforating canals with a diameter of 1 mm were added, a central opening with a diameter of 10 mm created in the circular implant part corresponding to the medullary canal for tibia reconstruction. The resulting STL-format models were loaded into the custom-made 3D printer software.

2.2 Post-treatment of 3D printed implants

3D printed samples were supplied for the post-treatment into biomimetic solution, which was produced by dissolving 115 g of monoammonium phosphate ($NH_4H_2PO_4$) in 500 mL of distilled water at room temperature and pH value 4.1 ± 0.1. 3D printed samples were kept there at 40°C up to 168 h. After that, the samples were thoroughly washed in distilled water at least 10 times, dried in air at 37°C and placed in a second solution, which was prepared by dissolving 95.2 g of CH_3COONa in 700 mL of distilled water at 40°C and pH value 8.2 ± 0.2. 3D printed samples were again kept at 40°C up to 168 h, then washed in distilled water for at least 10 times and dried in air at 37°C[11]. All used reagents were purchased from Sigma-Aldrich (USA).

2.3 Characterization of 3D printed implants

The porosity, intergranular size, and specific surface area were studied by mercury porosimeter (TriStar 3000, Micromeritics, USA). The phase composition was analyzed by conventional X-ray diffraction (XRD) (Shimadzu XRD-6000, Japan), with Ni-filtered CuKα1 target, λ =1.54183 Å. The samples were scanned from 2θ =3° to 60° with a step size of 0.02° and a preset time of 5 s. Scanning electron microscope (SEM) (Tescan Vega II, Czech Republic) equipped with EDS analyzer, operating in secondary and backscattered electron modes, was used for investigation of surface morphology, microstructure, and chemical composition. For SEM analysis, all samples were sputter-coated before imaging with a 25 nm-thick gold layer to impart electrical conductivity to the specimen surfaces. Fourier transform infrared (FTIR) spectroscopy study was performed using an Infrared Spectroscopy microscope (Nicolet Avatar 330 FTIR spectrometer, UK) in transmission mode. FTIR data were recorded over the range of 4000 – 400 cm^{-1} with 128 scans. The compressive strength of the samples was evaluated in accordance with the ISO standard 83.100: Cellular materials. At least five samples for each experimental point were tested. The compression test was carried out using an Instron 5581 (Bucks, UK) testing machine operating at a crosshead speed of 1 mm × min^{-1}.

2.4 Plasmid DNA deposition on 3D printed implants

The supercoiled naked plasmid DNA encoding *VEGFA* gene, an active substance of "Neovasculgen," the drug indicated for the treatment of patients with chronic lower limb ischemia (developed and certified for clinical applications by PJSC Institute of Human Stem Cells, Russia), was used to create personalized gene-activated implants[13]. Plasmid DNA carrying the gene of luciferase (*Luc*) was also used in our experiments to evaluate the transfection efficacy *in vivo*. The combination of 3D printed bone substitute with plasmid DNA was performed under previously developed protocol[14]. Briefly, 3D printed scaffolds were washed in a 0.5 M solution of sodium phosphate monobasic dihydrate ($NaH_2PO_4 \times 2H_2O$, Chimmed, Russia) at 37°C when constantly shaken for 10 h, washed in 1 ml of 10 mM $NaH_2PO_4 \times 2H_2O$ at 37°C when constantly shaken 4 times for 10 min, then were left at 37°C for 10 h until dried. After that, the samples were placed in a 10 mM $NaH_2PO_4 \times 2H_2O$ solution with plasmid DNA in the concentration of 1 μg/μl and incubated at 37°C and constant shaking for 10 h, and then a non-bound fraction of gene constructs was washed with 5 mM $NaH_2PO_4 \times 2H_2O$.

The binding of plasmid DNA with OCP surface was controlled visually by SEM and chemically when a bound plasmid DNA fraction was taken off with 0.5 M $NaH_2PO_4 \times 2H_2O$, and its concentration in a solution was measured with fluorometer Qubit 2.0 (Invitrogen, USA).

2.5 *In vivo* experiments

Animal trials were carried out in accordance with institutional guidelines/protocols in agreement with national laws and policies for animal care. The guidelines were approved by PJSC Institute of Human Stem Cells, Moscow, Russia.

2.5.1 Biodegradation assessment

Biodegradation assessment of 3D printed OCP based and gene-activated implants were studied in male rats with a body weight of 150 g (n = 24). A 15-mm median skin incision was done in the lower back under inflatration anesthesia with Sol. Lidocaini 1 – 2 ml and intramuscular sedation with Sol. Zoletili 100 – 10 mg/kg and 20 mm subcutaneous pockets were formed on both sides of the incision. The gene-activated bone substitutes were implanted into the right zone, but 3D printed scaffolds without plasmid DNA – into the left one. A post-operative wound was sutured by interrupted stitches with Polysorb 5/0. The animals were sacrificed in 15, 30, 90, 120, and 180 days by overdosage of Sol. Zoletili 100. The materials were extracted and fixed in 10% neutral formalin. Micro CT of the samples was performed by Brucker SKYSCAN 1174 (Belgium) and then the images were 3D-reconstructred using VG Studio Max software (Germany). A diameter, shape, and a surface area to implant volume ratio were determined. After decalcification in a Biodec-R solution (Bio-optica, Italy), histological slices were prepared under a standard procedure followed by hematoxylin and eosin staining.

2.5.2 Gene constructs delivery assessment *in vivo*

Balb/c mice with a body weight of 30 g (n = 20) were used in this experiment. 3D printed scaffolds (Control 1), 3D printed gene-activated implants with *VEGFA*-carrying (Control 2) or *Luc*-carrying plasmid DNA (test group) were inserted subcutaneously to an animal. Shame-operated animals (Control 3) and those injected with a solution of plasmid DNA with *Luc* gene (Control 4) were used as additional controls. On days 1, 7, 14, and 28, D-luciferin sodium salt (Lumtec, Russia) was intraperitoneally injected to animals which had been preliminarily sedated with Sol. Zoletili 100 – 10 mg/kg. In 10 min, they were placed in a bioluminometer IVIS Spectrum chamber (PerkinElmer, Inc., USA), and a luminescent signal was recorded for 1 min.

2.5.3 Segmental bone defect reconstruction

Male pigs with an average body weight of 50 ± 2 kg (n = 4) were used in this study. Each animal underwent surgery on the right tibia and the mandible on both sides under combined endotracheal anesthesia. After the surgery, all animals received antibiotic therapy (Cefazolin-natrii 1.0) for 7 days and then were sacrificed by thiopental sodium overdosage when sedated with Sol. Zoletili 100 in 3- and 6-months post-surgery. The bones with the previous surgery areas were resected. Reconstructive plates and screws were removed from the tibia; the metal constructions were left in the mandible to retain the regeneration integrity. The materials were fixed in 10% neutral formalin.

Tibia reconstruction: 10-cm straight incision was made through the skin along the anterior tibia surface, soft tissues were dissected, the diaphysis exposed subperiosteally and a T-shaped fragment corresponding to a planned bone defect with a total length of 30 mm was resected. 3D printed gene-activated implant was inserted into the defect, and osteosynthesis performed with the use of a 3.2 mm-thick reconstructive plate and screws with a diameter of 3.7 mm, some of them were fixed bicortically. Bone fragments were fixed stable on a surgical table. The post-operative wounds were closed in four layers with Polysorb 4/0, SurgiPro 4/0.

Mandible reconstruction: the intervention was carried out on both sides of the mandible under the same protocol. A skin linear incision was made

2 cm below and in parallel to the lower edge of the mandible from its angle by 4 cm forward, soft tissues were dissected, a surface of the mandibular body exposed subperiosteally. Osteotomy was performed by removing a lower edge fragment sized 25 × 15 × 10 mm^3 and retaining the mandible continuity. 3D printed gene-activated implant was fixed on the right side and plasmid-free 3D printed implant (as control) fixed on the left one within the defect using a straight titanium miniplate and miniscrews (a diameter of 2 mm, a length of 5 – 7 mm). The post-operative wounds were closed in four layers with Polysorb 4/0, SurgiPro 4/0.

CT: Having been fixed for 5 days, the materials were examined with medical CT in the same scanning mode and parameters, i.e. voxel size 0.08 mm, 80 kV, and 2 mA. The images were analyzed with standard tools in the Planmeca Romexis viewer software (Planmeca Oy, Finland). A quantitative assay of the images involved the determination of newly formed tissues density (in Hounsfield units (HU)) in three projections with apply of a region of interest tool and sizes of the remaining implants.

SEM: The bone fragments lengthwise through the central axis were cut. Several samples sized 5 × 5 × 5 mm^3 were resected from each part of every material from the border between the implant and a bone edge and from an implant central zone for SEM study. The remaining materials were used for a histologic examination. SEM study was performed after standard sampling with gold sputtering (section 2.3). Changes in the experimental samples' structure, chemical compositions, and the border between the implant and newly formed bone were evaluated.

Histological analysis: 5-μm thick slices were prepared from intact parts of every material without previous decalcification and stained with trichrome. The materials sampled for SEM were decalcified in a Biodec-R solution and used for histological specimens' preparation under the standard protocol with hematoxylin and eosin staining. All specimens were scanned in a Mirax Scanner (Carl Zeiss, Germany), and digital images were generated and evaluated qualitatively and quantitatively in the Panoramic Viewer (3DHistech Ltd, USA).

2.6 Statistical analysis

All results are expressed as mean±SD. Mann–Whitney U-test was used to compare independent groups, with Wilcoxon signed-rank test used for intra-group comparisons for each time points. $P < 0.05$ was considered statistically significant.

3 Results

All initial implants were produced by our modified 3D printing technology[11,12] of ceramic constructions from a synthesized TCP powder and 1.0% aqueous solution of phosphoric acid salt as described above. Experimental samples set reproduced a shape, sizes and the structure of CAD (computer assisted design) STL-models with a high (ca. ± 100 μm) spatial accuracy and comprised: 1) non-porous disks to assess biodegradation; 2) porous disks to evaluate a level of plasmid DNA delivery; and 3) complex custom-made implants to reconstruct the tibia and mandible large defects in pigs.

3D printing fusing of TCP agglomerated particles and "ink" (diluted phosphoric acid) is based on a hydraulic setting reaction leading to formation of dicalcium phosphate dihydrate (DCPD), and thus, to layer-crossing bonding of the powder. Finally, 3D structure is formed. According to the XRD analysis, the 3D printed samples compose of unreacted TCP and certain amounts of DCPD (**Figure 2A**). FTIR and SEM data of the experimental samples confirmed the formation of DCPD (**Figure 2B and C**). SEM analysis of the 3D printed samples are shown in **Figure 2C**. Particles was about 5 – 20 μm in dimension. The DCPD crystals had a flower-like morphology. The width of the DCPD crystals was in the range of 1 – 50 μm, and their thickness was few microns.

Compressive strength of the 3D printed samples is presented on **Figure 2F** and was in the range of 1.5 – 4.5 MPa, depending on the number of micro-drops from printing head.

The post-treatment of the 3D printed samples lead to formation of OCP phase and the adhesive

effect between particles. The crystallization of TCP to DCPD was finished after 7 days (**Figure 2A and B**). 3D printed samples with DCPD phase composition were transformed into OCP of soaking in sodium acetate, according to XRD, FTIR and SEM (**Figure 2A, B and D**). XRD data of the OCP showed certain amounts of OCP phase with (100) reflection at 2θ=4.9°. However, the post-treated samples contained some quantity of unreacted DCPD. High intensity of diffraction peaks indicates high crystallinity of OCP materials (**Figure 2A**). FTIR data of the OCP samples are presented on **Figure 2B** and are in agreement with those previously reported in Fowler *et al*.[15]. The OH bending modes originating from the HPO_4 groups of OCP were observed at 1295 cm^{-1}. P–O in HPO_4 and PO_4 groups were assigned at 1118, 1029, and 960 cm^{-1}. The P–OH stretching mode of HPO_4 groups was at 870 cm^{-1}. OCP plates were needle-like 2 – 5 μm long and 1 – 2 μm wide (**Figure 2D**).

Compressive strength of 3D printed samples is presented in **Figure 2F and G**. The strength of the investigated samples increased from 1.5 to 4.5 MPa up to about 4.3 – 7.9 MPa after post treatment.

3D printed gene-activated implants were produced using the supercoiled naked plasmid DNA encoding *VEGFA* gene. Based on the SEM study, we identified some round structures on the surface of gene-activated bone substitutes, which corresponded to plasmid DNA macromolecules (**Figure 3A and B**). Fluorimetry results demonstrated an average concentration of 3D scaffold-bound plasmid DNA to be 52.74 ± 1.76 ng/mg.

A luminescent signal with intensity corresponding to the production level of luciferase encoded by pDNA-*Luc* was detected only locally – within a zone of localization of a pDNA-*Luc* solution or 3D printed gene-activated implants containing pDNA-*Luc*. No signal was detected in

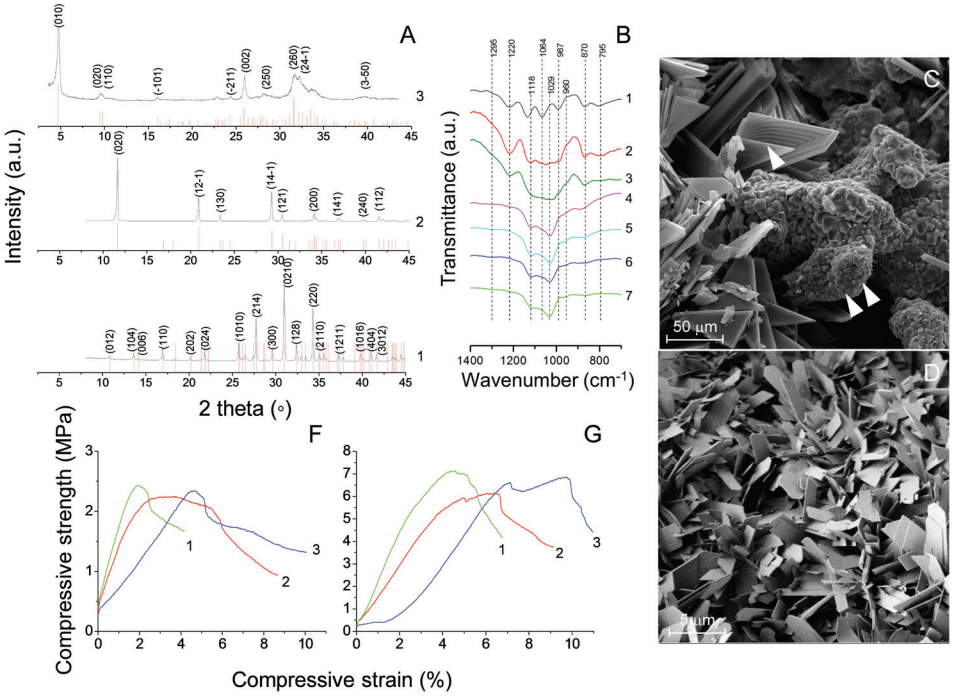

Figure 2. (A) XRD data of the formation of 3D printed TCP (1) to DCPD samples soaked in calcium nitrate solution during 7 days (2) and to OCP samples in sodium acetate during 7 days (3). (B) FTIR data of the formation of 3D printed samples soaked in calcium nitrate solution after 7 days (1) and samples in sodium acetate after 1 (2); 2 (3); 3 (4); 5 (5); 6 (6) and 7 (7) days. (C, D) SEM images of 3D printed samples. (F, G) Compressive strength of 3D printed samples before and after chemical treatment.

other animal body parts or groups. A luminescence level peaked on day 1 after a subcutaneous injection to mice in the control group 4, with its being the lowest intensity in the test group. Later on, the signal intensity gradually decreased in the control 4, while peaking on day 7 with a subsequent smooth reduction in the test group. Intergroup comparison showed the signal level to be significantly higher in the control 4 only 1 day after surgery, with it being higher in the test group on days 7 – 28. The peak signal intensity value in the group with 3D printed gene-activated implants was 1.9-fold of a maximum value in the control group (**Figure 3C**). The others control groups (1-3) showed no luminiscent signal.

The initial diameter, volume, and the "surface-to-volume" ratio of 3D printed disks was 10.1 ± 0.2 mm, 116.53 ± 8.16 mm^3, and

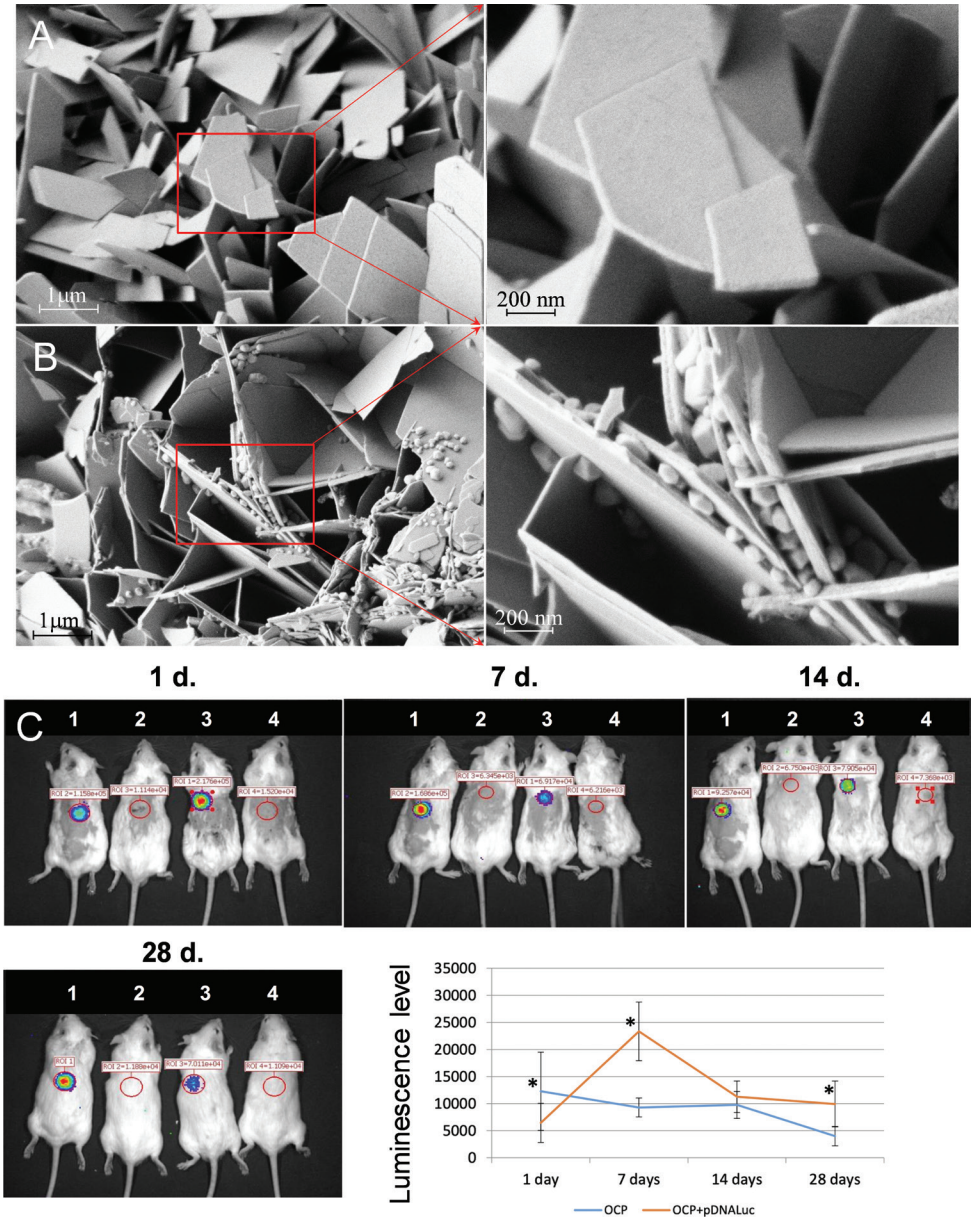

Figure 3. SEM images of 3D printed OCP implants (A) and gene-activated implants (B). (C) Plasmid DNA delivery from 3D printed OCP implants in subcutaneous *in vivo* test, bioluminescent study. (1) test group, (2) OCP implant without pDNA-*Luc*, (3) solution with pDNA-*Luc*, (4) OCP implant with pDNA-*VEGF*. *differences between the group are statistically significant, $P < 0.05$.

0.002, respectively. Materials resorbed form their surfaces and within a zone of the direct contact to soft tissues. The diameter and volume gradually reduced and the "surface-to-volume" ratio increased both in 3D printed scaffolds and gene-activated implants. An average diameter decreased more intensively with an abrupt drop by day 40 and a subsequent stabilization and a smooth decline in the test group, while its change being almost linear in the control group. There was a two-fold volume reduction by day 60 in both groups (**Figure 4**).

We found no histological signs of inflammation in the area of 3D printed OCP (control) implantation. Since day 15, a highly vascularized connective tissue capsule with a thickness of 50 – 70 μm formed around implants. However, cellular and tissue elements did not penetrate into OCP structure. Starting from day 45, in some parts of the implants there were defects in the structure, their number and size gradually increased by day 180 by forming "cavities of dissolution" with a diameter of 30 – 50 μm and scalloped edges that indicated biodegradation. There were no multinucleated foreign bony giant cells. On day 180 after implantation, connective tissue grew inside the implants to 50 – 70 μm from a surface (**Figure 4**).

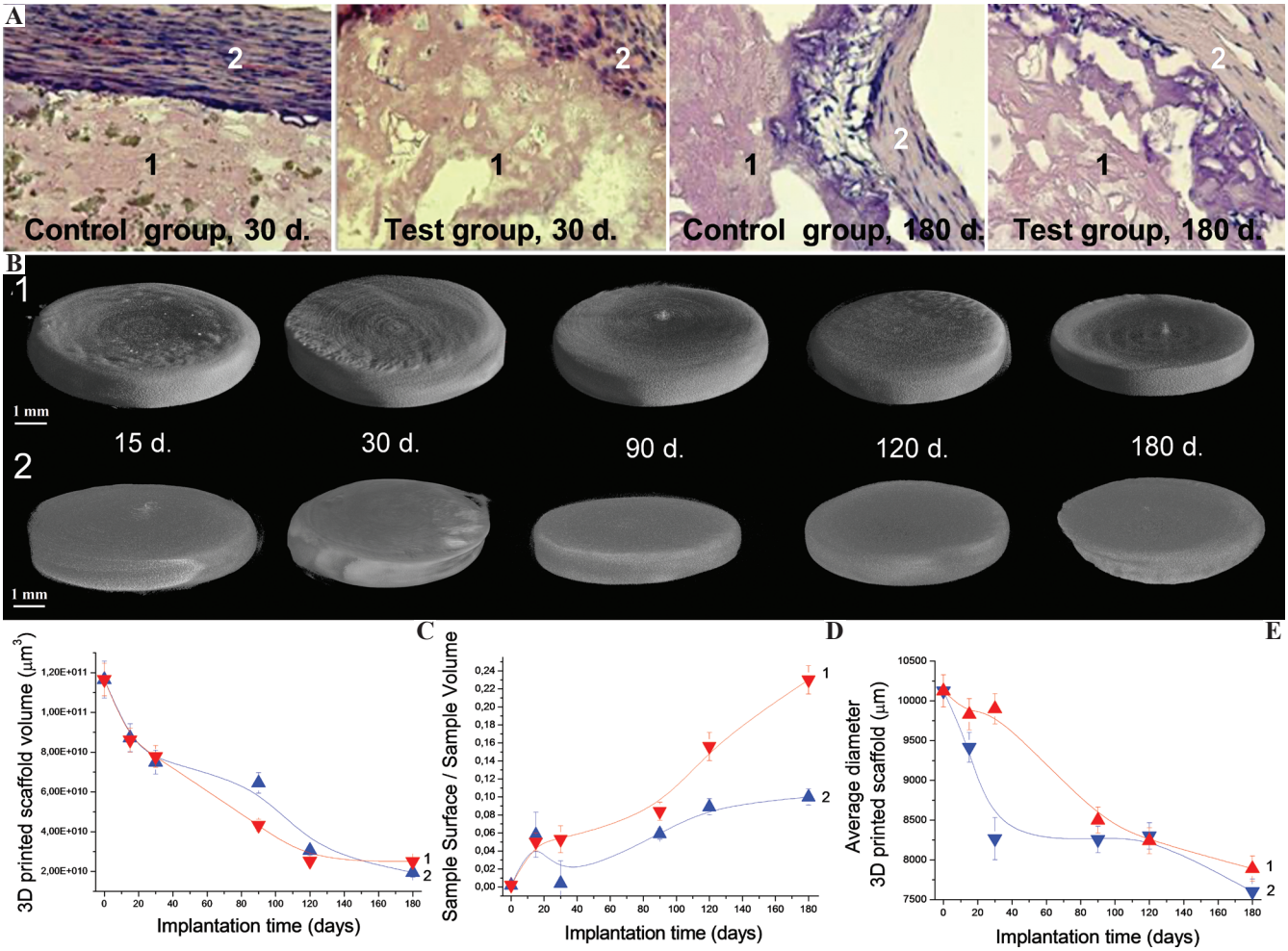

Figure 4. 3D printed OCP-based-(control group) and gene-activated (test group) implants in subcutaneous *in vivo* test, biodegradation study. (A) Histological analysis: (1) implants, (2) fibrous tissue; (B) 3D microCT images (1) (control (up) and (2) test (down) groups); (C, D, F) Kinetic of biodegradation parameters: red – control group (1); blue – test group (2). *differences between the group are statistically significant, $P < 0.05$.

The biodegradation study of personalized gene-activated constructs demonstrated implants structure disintegration and connective tissue growing into them from day 15 after implantation. A capsule covering the implants included active fibroblasts and was intensively vascularized with a larger number of blood vessels than in the control group ($P = 0.021$). In 45 – 120 days, we found a further structure disintegration and thinning of 3D printed gene-activated implant edges. Later on, all implants were highly porous: optically empty vacuoles occupied a significant volume (about 60%), their diameter achieved 200 – 250 μm. Connective tissue in-grew to a depth of 100 – 150 μm (**Figure 4**). As in the control, there were no signs of inflammation. In general, personalized gene-activated materials possessed a profile of more evident bioresorption and a slightly higher rate of biodegradation.

None of animals died during the experiment until a planned sacrifice. Wounds healed in three animals without abnormalities in 10 days after surgery. Since that time the animals started resting on the operated limb; one animal had a post-operative wound infection after tibia reconstruction.

Based on CT findings, the tibia integrity was restored in all cases, and implants integrated with bone fragments without forming a connective tissue capsule. Bone thickness increased within the area of intervention due to a pronounced periosteal callus; its diameter achieved 31.5 and 40.3 mm in the greatest dimension in 3 and 6 months after surgery, respectively, with an initial diameter of being <20 mm. The implants retained their initial shape with structure becoming heteromorphic. In addition to canals filled with newly formed tissues of bone density, we detected some cracks without fragment disintegration in the implant structure (**Figure 5**). The implants length reduced to 26 and 24 mm, whereas their diameter to 15 and 14 mm in 3 and 6 months after surgery, respectively. An average tissue density within a tibia reconstruction zone was 1362 ± 617.6 HU in 3 months and 1332 ± 572.2 HU in 6 months, with the initial implant density of more than 2000 HU.

Optimal osteointegration was confirmed by SEM and a histologic examination. SEM results showed that a crystal structure of OCP-based scaffolds defused without a border between newly formed bone tissue and the implant. Calcium to phosphorus ratio (Ca/P) in the areas of 3D printed implants and newly formed bone tissue was 2.06 and 1.83 and 1.90 and 2.23 in 3 and 6 months after surgery, respectively.

Based on histological analysis, a gene-activated bone substitute surface contacted directly with a newly formed woven bone tissue without forming a connective tissue capsule in 3 months after surgery. There were both macropores corresponding to prefabricated canals and numerous micropores in the implant structure. Trabeculae of a newly formed bone tissue enlaced the implant, directly extending into macro- and micropores. Vascularized bone tissue had been growing from both periosteum and endosteum sides. Bone rods spread from the implant to a diaphysis wall in the form of bridges (**Figure 5**). Bone trabeculae arose directly from the implant both in the periphery and in its depth; newly formed trabeculae adhered to a rarefied implant surface, their side contacting with the material had irregular edge, an opposite side was characterized by a smooth surface with osteoblasts and bone lining cells involved. Fusing trabeculae of newly formed bone tissue constituted a mesh structure, neither evidence of woven bone remodeling into lamellar tissue, nor osteoclastic resorbtions occurred at this time point. A fibrous tissue was detected only within inter-trabecular spaces. A newly formed diaphysis wall consisted of a spongy bone with bone marrow elements in inter-trabecular spaces. There was a pronounced periosteal response with woven bone tissue trabeculae formation within basal regions of the periosteum.

In 6 months after surgery, personalized gene-activated bone substitutes were completely integrated into the tibia proximal and distal fragments and significantly rarefied around initial perforations. Macro- and micropores as well as a peripheral implant surface were covered with trabeculae of a newly formed bone tissue. By this time point, the bone tissue directly in implant perforations as well as along its perimeter remodeled into lamellar forming osteons even in the implant macropores. There were no cells responsible for

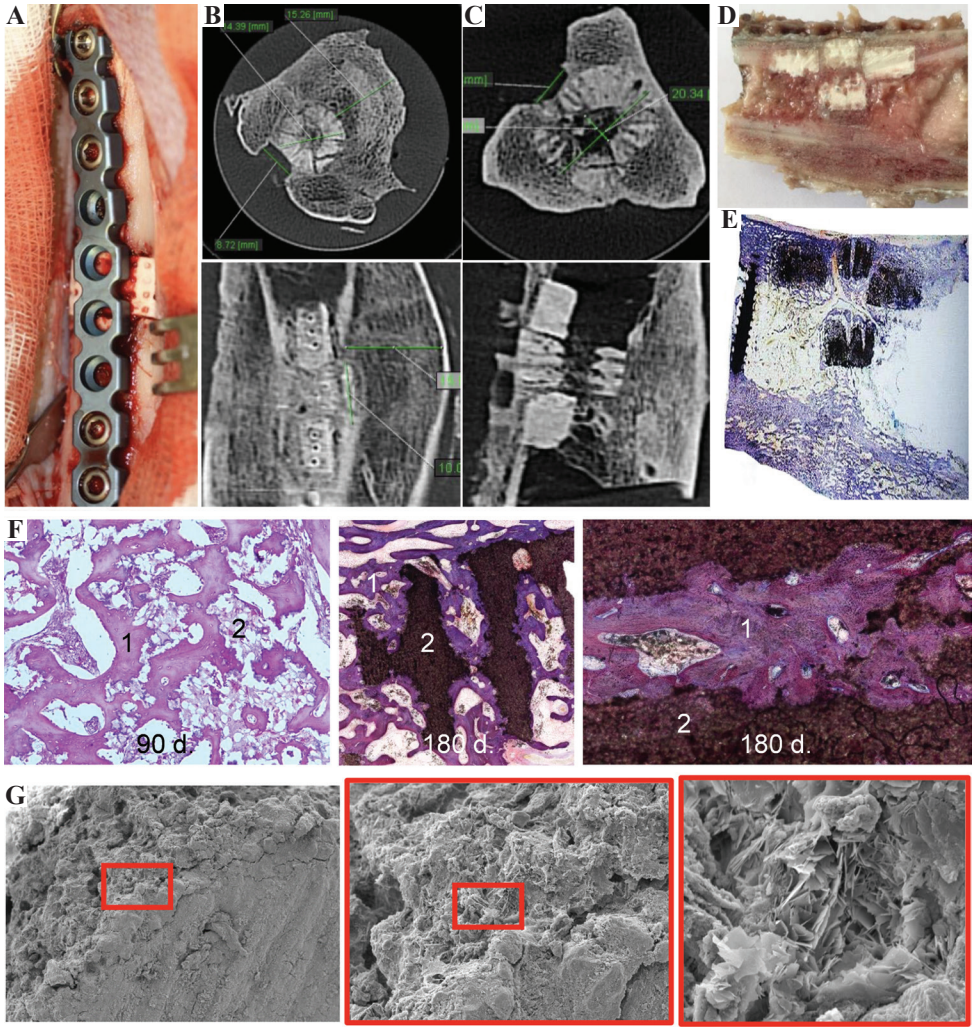

Figure 5. Tibia reconstructed with 3D printed gene-activated implants. (A) Intraoperation view; (B, C) CT scans in 3 and 6 months, respectively; (D) Longitudinal slice of the tibia with bone grafting zone; (E) Non-decalcified histological slice; (F) Histological analysis in 3 and 6 months after surgery: (1) newly formed bone tissue, (2) partially resorbed implant; (G) SEM images.

material resorption or bone tissue remodeling. Inter-trabecular spaces were filled with properly vascularized bone marrow (**Figure 5**).

As in case of long (tubular) bones the mandible integrity restored on both sides, the implants fully integrated with bone defect walls. There was no border between the implant and a bone defect wall in some regions, especially in 6 months after surgery. No hypertrophic periosteal callus formed. All sizes of both plasmid-free and gene-activated 3D printed implants reduced by, on average, 1 mm in 3 months and 2 mm in 6 months after surgery. Mean tissue densities within the zone of the mandibular reconstruction in 3 and 6 months after surgery were 1972 ± 397.5 HU and 1974 ± 368.5 HU in the control group and 1925 ± 289.2 HU and 1986 ± 390.1 HU in the test group, respectively.

As in the tibia reconstruction, optimal osteointegration was confirmed by SEM. Ca/P ratios in the areas of 3D printed implants and newly formed bone tissue were: in the test group, 2.07 – 2.11 and 2.16 – 2.74 in 3 and 6 months after surgery, respectively; in the control group, 1.95 – 2.26 and 1.87 – 1.94 at 3 and 6 month time points.

According to the histological analysis, the gene-activated implants were integrated with

the mandible in 3 months after surgery; irregular implant surface was directly surrounded by a newly formed bone tissue of a mixed structure (woven and lamellar) without a connective tissue capsule. There was a typical tendency for osteon-like structures and circular trabeculae to be formed. There were no cells on the surface of bone trabeculae in contact with the bone substitute, while active osteoblasts detected on the opposite side. There were evident signs of periosteal osteoblasts were nearby the zone of implantation (**Figure 6**). A richly vascularized connective tissue was detected in inter-trabecular spaces. No cellular or tissue structures were identified in the implant central zones. There were single osteoclasts on a newly formed bone trabeculae surface on the side of connective tissue. A similar picture was observed in 3D printed OCP implants without gene

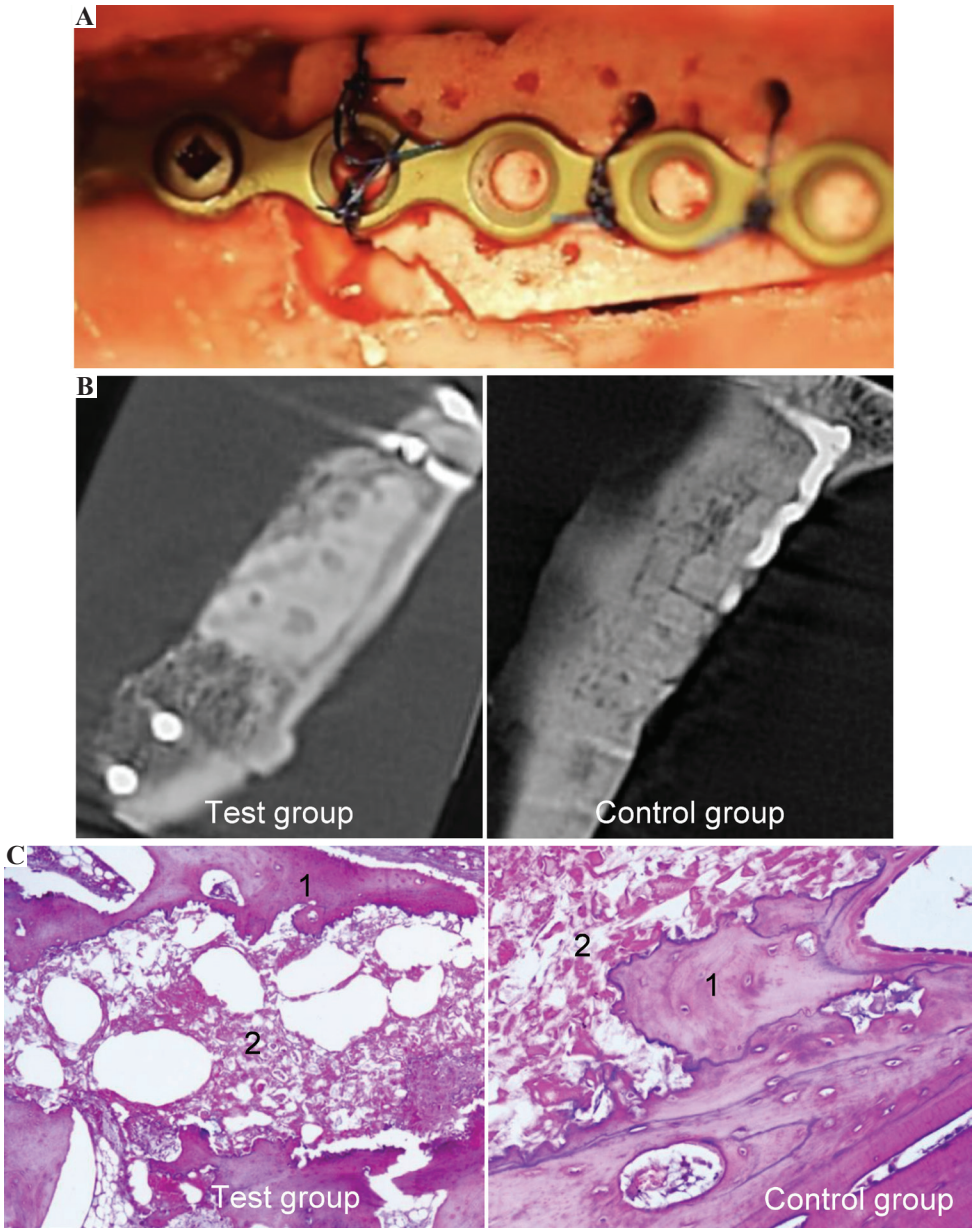

Figure 6. Mandible reconstructed with 3D printed OCP implants and gene-activated implants. (A) Intraoperation view; (B) CT scans in 6 months after surgery; (C) Histological analysis in 6 months after surgery: (1) newly formed bone tissue; (2) partially resorbed implant.

constructs; however, periosteal osteogenesis was less evident.

In 6 months after implantation, the peripheral part of gene-activated materials was actively substituted with bone tissue. A border with the implant along its entire length was composed of newly formed bone tissue trabeculae **(Figure 6)** without fibrous tissue. A woven bone tissue remodeled into lamellar tissue. The implant surface was rarefied and had a great number of optically empty cavities sized to 300 μm. Still, no cellular and tissue elements extended into the material. There were no cellular signs of osteoclastic resorption. Inter-trabecular spaces were in part colonized with hematopoietic bone marrow. There was an optimal osteointegration in 3D printed OCP implants with similar dynamics of bone tissue rearrangement into lamellar tissue; however, the colonization of inter-trabecular spaces with blood-forming (hematopoietic) bone marrow was less active.

4 Discussion

Bone reconstructive surgery in traumatology and orthopedics, neurosurgery, oral and maxillofacial surgery still remains challenging. Small defects can be managed with the use of osteoconductive bone substitutes, including a combination with "improvised" techniques for biologic activity enhancement such as mixing with autologous bone fragments, platelet-, or growth factor-enriched plasma, etc. However, large/critical size bone defects and alveolar ridge atrophy of significant size are characterized by "osteogenic insufficiency," a loss of cambial cellular elements and/or factors, invloved in bone regeneration, therefore intensive osteoinduction is required[9].

Additive manufacturing or 3D printing techniques provide substantial opportunities for effective personalized treatment of patients with large bone defects. However, to overcome osteogenic insufficiency, custom-made implants should be combined with osteogenesis-stimulating factors such as living cells, growth factors, or gene constructs that encode them. 3D bioprinting of tissue-engineered constructs are most intensively developed, probably due to the attractive idea to create a fully functional tissue or organ *ex vivo* for subsequent clinical transplantation[6,10,16,17] or for usage as an *in vitro* model to study the disease pathogenesis and drugs development[18]. However, in addition to well-known technological problems, tissue engineering is associated with high costs and considerable difficulties in clinical translation from a regulatory point of view[9]. Furthermore, additive manufacturing is actively used to produce personalized bone implants with growth factors[19,20]. However, protein molecules, being short-lived, and short-distant, cannot exhibit their full biological effect.

Although 3D bioprinting has become more complex in an attempt to combine different approaches[21], there is a search for simpler alternatives that involves, for instance, the use of gene constructs for creating personalized bone substitutes. Despite significant advances in the research of standardized gene-activated matrices[22-24] and additive manufacturing technologies for bone grafting, to date there are only a few studies related with personalized gene-activated tissue substitutes[25,26], and none of them described calcium phosphate-based ceramic being used as a scaffold without any hydrogels or other materials that are easy to be printed.

Based on our previous results in OCP studies[27], 3D printing of OCP-based implants[11] and standardized gene-activated materials[23,28], we have started the development of a personalized gene-activated bone substitute based on the OCP and plasmid DNA that delivers *VEGFA* gene, applicable for large bone defects substitution and guided bone regeneration. We expected the increased level of *VEGFA* to promote angiogenesis and reparative osteogenesis. Moreover, a direct stimulating effects of *VEGF* on proliferation and differentiation of bone cells[29] and non-canonic intracrine effects specific for a VEGF gene transfer[30] were described. Additional prerequisites to use this gene construct in the study were our previously obtained clinical data on a successful treatment of a patient with mandibular non-unions with the use of a gene-activated material, delivering *VEGFA*[28].

First, in our work, we have realized a combination and further development of the processes involving chemical interaction between TCP agglomerated particles and "ink" based on diluted phosphoric acid, followed by chemical post-treatment of the printed DCPD structure at physiological temperatures[11]. DCPD structure can be further transformed into OCP phase. **Figure 7** presents a schematic overview of the proposed mechanism of OCP-based 3D printed scaffolds production. It can be established: in the initial stage (3D printing), the pH value was low due to the presence of phosphoric acid, and the reaction between $Ca_3(PO_4)_2$ and H_3O^+ yielded Ca^{2+} ions. The Ca^{2+} ions reacted with HPO_2^{-4} ions, which formed $CaHPO_4 \times 2H_2O$. The further increase of the pH value of the solution during the post-treatment process leads to OCP nucleation and growth.

The next task of the present work involved the production of gene-activated implants based on the OCP and plasmid DNA with *VEGFA* gene. According to fluorimetry data, the concentration of plasmid DNA bound to 3D printed scaffolds was 52.74 ± 1.76 ng/mg that correlated with our previous findings related with OCP granule-based bone substitute[32].

To evaluate intrinsic biodegradation rate of the material we have made non-porous OCP-based disk-shaped implants, since macro- and micropores unavoidably accelerate biodegradation of the scaffolds. Obtained data could be used as a reference value in the further studies of porous implants. At the same time, the presence of plasmid DNA almost did not affect the rate of this process.

A delivery of gene constructs, which does not exceed 1% in case of naked plasmid DNA,

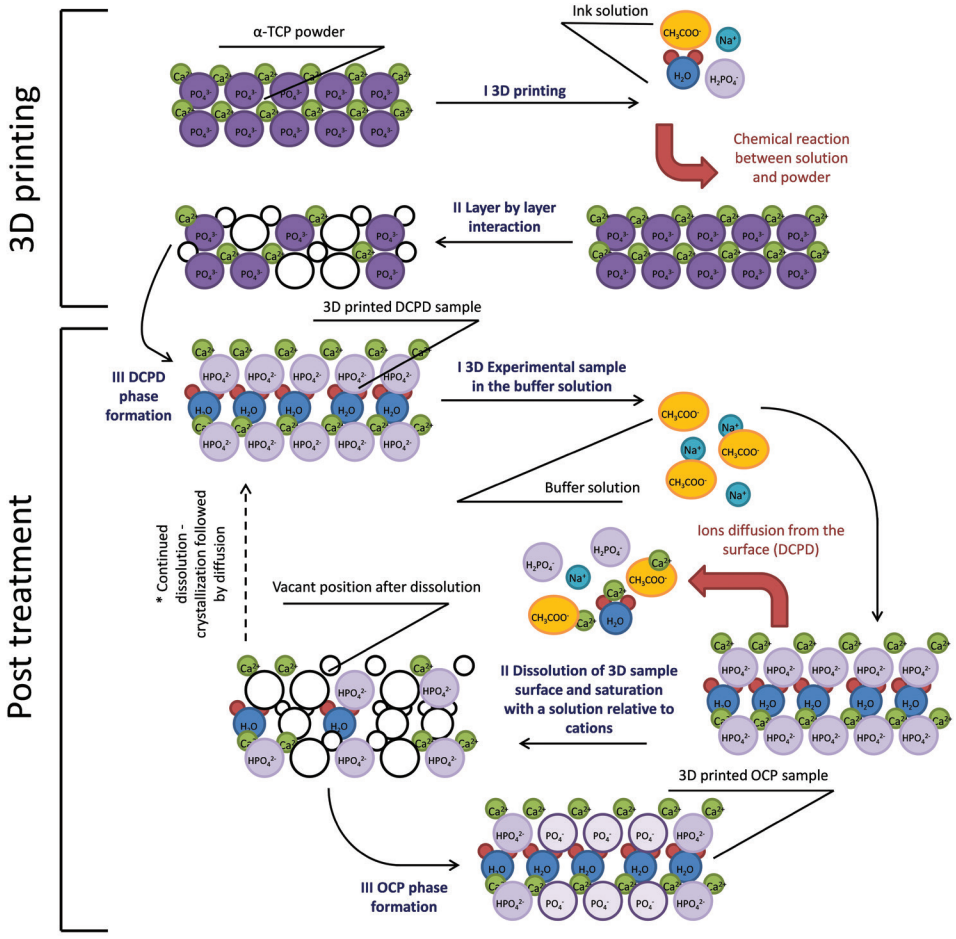

Figure 7. Schematic overview of the 3D printing and biomimetic post-treatment.

is the main challenge of gene-activated matrix approach[32]. However, in our study, we have detected a high prolonged level of plasmid DNA delivery *in vivo* that might be caused by a positive effect of 3D printed OCP-based scaffold. Indeed, some authors suggested this effect for calcium phosphate matrixes[33] that could be a peculiar extrapolation of well-known calcium phosphate method used to increase plasmid DNA transfection *in vitro*.

An osteoinductive effect of pDNA-*VEGFA* along with the osteoconductive effect of the OCP scaffold facilitated the restoration of bone integrity in pigs. Moreover, morphological and structural changes of 3D printed implants and their effects on adjacent tissues had similar features both in tibia and mandibular reconstruction. Materials form test and control groups were characterized by optimal osteointegration capability, since there was no fibrous tissue encapsulation of the scaffold. A newly formed bone tissue followed the implant topography filling in all irregularities and pores. One of the peculiarities was that rapid woven bone remodeled led into a lamellar tissue occuping almost the entire volume of the newly formed bone tissue in 6 months after surgery. At the latest time point, the 3D printed materials became more porous. However, a half-resorption period for OCP-based implants of that structure was not achieved in this study. In addition, sites of cartilaginous callus formation, which are specific for bones with enchondral ossification were not detected after tibia reconstruction that might be caused by osteoinductive effects mediated by angiogenesis stimulation. Increased angiogenesis could made the reparative process to bypass a cartilaginous callus stage at all or at least accelerate it with cartilaginous tissue replacement by bone before 3-month time point. Moreover, there was hematopoietic bone marrow formation within the inter-trabecular spaces at the 1st time point.

5 Conclusions

In our work, 3D personalized gene-activated bone substitutes, based on the OCP and pDNA-*VEGFA*, have been developed and produced with the use of 3D printing technology for the first time. The safety of bioactive materials, a high level of plasmid DNA delivery in cells *in vivo* and the efficacy of large segmental bone defects substitution with and without pDNA-*VEGFA* loading have been confirmed experimentally. The results of our study demonstrated that combination of gene therapy and 3D printing with biomimetic post-treatment is an effective approach to overcome current limitations in production of personalized implants for critical size bone defect reconstruction.

Authors' contributions

Ilya Y. Bozo: Methodology, Investigation, Writing - Original Draft. Roman V. Deev: Study Design, Data Analysis. Igor V. Smirnov: Investigation, Visualization. Alexander Yu. Fedotov: Investigation. Vladimir K. Popov: 3D Printing Methodology Development, Original Draft Writing. Anton V. Mironov: Investigation. Olga A. Mironova: 3D Printing Software Development. Alexander Yu. Gerasimenko: Investigation. Vladimir S. Komlev: Conceptualization, Methodology, Writing - Reviewing and Editing, Visualization, Supervision. The manuscript was written through contributions of all authors. All authors have given approval to the final version of the manuscript.

Acknowledgment

This work was supported by the Ministry of Science and Higher Education within the State Assignment FSRC "Crystallography and Photonics" RAS in the part of 3D modeling of implants with predefined architecture and the Russian Foundation for Basic Research (grants no.18-29-11081 mk) in the part of the development of gene-activated materials. The authors acknowledge deep gratitude to M. Mavlikeev, A. Titova, A. Bilyalov, and M. Abyzova for their participation in the studies of gene construct delivery and to P.A. Makarevich for providing pDNA-*Luc* and to A.E. Baranchikov for high resolution SEM study.

Conflicts of Interest

The authors declare that they have no conflicts of interest.

References

1. Number of All-listed Procedures for Discharges from Shortly-stay Hospitals, 2010. Available from: http//www.cdc.gov/nchs/data/nhds/10Detaileddiagnosesprocedures/2010det10_alllistedprocedures.pdf. [Last accessed on 2020 March 01].
2. Rogers GF, Greene AK, 2017, Autogenous Bone Graft: Basic Science and Clinical Implications. *J Craniofac Surg*, 23:323–7.
3. Hernandez I, Kumar A, Joddar B, 2017, A Bioactive Hydrogel and 3D-Printed Polycaprolactone System for Bone Tissue Engineering. *Gels*, 3:26.DOI: 10.3390/gels3030026.
4. Ge Z, Tian X, Heng BC, *et al*., 2009, Histological Evaluation of Osteogenesis of 3D-Printed Poly-lactic-co-glycolic Acid (PLGA) Scaffolds in a Rabbit Model. *Biomed Mater*, 4:021001.DOI: 10.1088/1748-6041/4/2/021001.
5. Shim JH, Kim SE, Park JY, *et al*., 2014, Three-dimensional Printing of rhBMP-2-loaded Scaffolds with Long-term Delivery for Enhanced Bone Regeneration in a Rabbit Diaphyseal Defect. *Tissue Eng Part A*, 20:1980–92.DOI: 10.1089/ten.tea.2013.0513.
6. Ahlfeld T, Doberenz F, Kilian D, *et al*., 2018, Bioprinting of Mineralized Constructs Utilizing Multichannel Plotting of a Self-setting Calcium Phosphate Cement and a Cell-laden Bioink. *Biofabrication*, 10:045002. DOI: 10.1088/1758-5090/aad36d.
7. Dorozhkin SV, 2009, Calcium Orthophosphates in Nature Biology and Medicine. *Materials*, 2:399–498.DOI: 10.3390/ma2020399.
8. Liu Y, Cooper PR, Barralet JE, *et al*., 2007, Influence of Calcium Phosphate Crystal Assemblies on the Proliferation and Osteogenic Gene Expression of Rat Bone Marrow Stromal Cells. *Biomaterials*, 28:1393–1403.DOI: 10.1016/j.biomaterials.2006.11.019.
9. Deev RV, Drobyshev AY, Bozo IY, *et al.*, 2015, Ordinary and Activated Bone Grafts: Applied Classification and the Main Features. *Biomed Res Int*, 2015:365050.DOI: 10.1155/2015/365050.
10. Murphy SV, Atala A, 2014, 3D Bioprinting of Tissues and Organs. *Nat Biotechnol*, 32:773–85.DOI: 10.1038/nbt.2958.
11. Komlev VS, Popov VK, Mironov AV, *et al*., 2015, 3D Printing of Octacalcium Phosphate Bone Substitutes. *Front Bioeng Biotechnol*, 3:81.
12. Barinov SM, Vakhrushev IV, Komlev VS, *et al*., 2015, 3D Printing of Ceramic Matrices for Engineering of Bone Tissue. *Inorg Mater*, 6:316–322.DOI: 10.1177/1074248415574336.
13. Deev RV, Bozo IY, Mzhavanadze ND, *et al*., 2015, pCMV-vegf165 Intramuscular Gene Transfer is an Effective Method of Treatment for Patients with Chronic Lower Limb Ischemia. *J Cardiovasc Pharmacol Ther*, 20:473–82.
14. Bozo IY, Komlev VS, Drobyshev AY, *et al*., 2015, Method for Creating a Personalized Gene-activated Implant for Regenerating Bone Tissue. Patent No. EP3130342.
15. Fowler BO, Marković M, Brown WE, 1993, Octacalcium Phosphate. 3. Infrared and Raman Vibrational Spectra. *Chem Mater*, 5:1417–23.DOI: 10.1021/cm00034a009.
16. Kang HW, Lee SJ, Ko IK, *et al*., 2016, A 3D Bioprinting System to Produce Human-scale Tissue Constructs with Structural Integrity. *Nat Biotechnol*, 34:312–9.DOI: 10.1038/nbt.3413.
17. Daly AC, Pitacco P, Nulty J, *et al*., 2018, 3D-printed Microchannel Networks to Direct Vascularisation during Endochondral Bone Repair. *Biomaterials*, 162:34–46.DOI: 10.1016/j.biomaterials.2018.01.057.
18. Lal H, Patralekh MK, 2018, 3D-Printing and its Applications in Orthopaedic Trauma: A Technological Marvel. *J Clin Orthop Trauma*, 9:260–8.DOI: 10.1016/j.jcot.2018.07.022.
19. Huang KH, Lin YH, Shie MY, *et al*., Effects of Bone Morphogenic Protein-2 Loaded on the 3D-Printed MesoCSScaffolds. *J Formos Med Assoc*, 117:879-87.DOI: 10.1016/j.jfma.2018.07.010.
20. Lee SJ, Lee D, Yoon TR, *et al*., 2016, Surface Modification of 3D-Printed Porous Scaffolds via Mussel-inspired Polydopamineand Effective Immobilization of rhBMP-2 to Promote Osteogenic Differentiation for Bone Tissue Engineering. *Acta Biomater*, 40:182–191.DOI: 10.1016/j.actbio.2016.02.006.
21. Du M, Chen B, Meng Q, *et al*., 2015, 3D Bioprinting of BMSC-laden Methacrylamide Gelatin Scaffolds with CBD-BMP2-collagen Microfibers. *Biofabrication*, 7:044104.DOI: 10.1088/1758-5090/7/4/044104.
22. Deev RV, Drobyshev RV, Bozo IY, *et al*., 2013, Construction and Biological Effect Evaluation of Gene-activated Osteoplastic Material with Human VEGF Gene. *Cell Transplant Tissue Eng*, 8:78–85.
23. Feichtinger GA, Hofmann AT, Slezak P, *et al*., 2014, Sonoporation Increases Therapeutic Efficacy of Inducible and Constitutive BMP2/7 *In Vivo* Gene Delivery. *Hum Gene Ther Methods*, 25:57–71.DOI: 10.1089/hgtb.2013.113.
24. Evans CH, Huard J, 2015, Gene Therapy Approaches to Regenerating the Musculoskeletal System. *Nat Rev Rheumatol*, 11:234–42.DOI: 10.1038/nrrheum.2015.28.
25. Cunniffe GM, Gonzalez-Fernandez T, Daly A, *et al*., 2017, Three-dimensional Bioprinting of Polycaprolactone Reinforced Gene Activated Bioinksfor Bone Tissue

Engineering. *Tissue Eng Part A*, 23:891–900.DOI: 10.1089/ten.tea.2016.0498.

26. Gonzalez-Fernandez T, Rathan S, Hobbs C, 2019, Pore-forming Bioinksto Enable Spatio-temporally Defined Gene Delivery in Bioprinted Tissues. *J Control Release*, 301:13–27.DOI: 10.1016/j.jconrel.2019.03.006.
27. Komlev VS, Barinov SM, Bozo IY, *et al*., 2014, Bioceramics Composed of Octacalcium Phosphate Demonstrate Enhanced Biological Behaviour. *ACS Appl Mater Interfaces*, 6:16610–20.DOI: 10.1021/am502583p.
28. Bozo IY, Deev RV, Drobyshev AY, *et al*., 2016, World's First Clinical Case of Gene-activated Bone Substitute Application. *Case Rep Dent*, 2016:8648949.DOI: 10.1155/2016/8648949.
29. Yang YQ, Tan YY, Wong R, *et al*., 2012, The Role of Vascular Endothelial Growth Factor in Ossification. *Int J Oral Sci*, 4:64–8.
30. Liu Y, Berendsen AD, Jia S, *et al*., 2012, Intracellular VEGF Regulates the Balance Between Osteoblast and Adipocyte Differentiation. *J Clin Invest*, 122:3101–13.DOI: 10.1172/jci61209.
31. Bozo IY, Deev RV, Drobyshev AY, *et al*., 2015, Efficacy of Gene-activated Osteoplastic Material Based on Octacalcium Phosphate and Plasmid DNA with VEGF Gene for Critical-sized Bone Defects Substitution. N.N. *Priorov Herald Traumatol Orthop, 1:35–42.DOI: 10.32414/0869-8678-2015-1-35-42.*
32. Schertzer JD, Plant DR, Lynch GS, 2006, Optimizing Plasmid-based Gene Transfer for Investigating Skeletal Muscle Structure and Function. *Mol Ther*, 13:795–803.DOI: 10.1016/j.ymthe.2005.09.019.
33. Keeney M, van den Beucken JJ, van der Kraan PM, *et al*., 2010, The Ability of a Collagen/Calcium Phosphate Scaffold to Act as its Own Vector for Gene Delivery and to Promote Bone Formation Via Transfection with VEGF (165). *Biomaterials*, 31:2893–902.DOI: 10.1016/j.biomaterials.2009.12.041.